
PREDICTIVE AUXILIARY OBJECTIVES IN DEEP RL MIMIC LEARNING IN THE BRAIN

Ching Fang

Center for Theoretical Neuroscience
Columbia University
New York, NY USA
ching.fang@columbia.edu

Kimberly Stachenfeld

Google DeepMind
Center for Theoretical Neuroscience
Columbia University
New York, NY USA
stachenfeld@deepmind.com

ABSTRACT

The ability to predict upcoming events has been hypothesized to comprise a key aspect of natural and machine cognition. This is supported by trends in deep reinforcement learning (RL), where self-supervised auxiliary objectives such as prediction are widely used to support representation learning and improve task performance. Here, we study the effects predictive auxiliary objectives have on representation learning across different modules of an RL system and how these mimic representational changes observed in the brain. We find that predictive objectives improve and stabilize learning particularly in resource-limited architectures, and we identify settings where longer predictive horizons better support representational transfer. Furthermore, we find that representational changes in this RL system bear a striking resemblance to changes in neural activity observed in the brain across various experiments. Specifically, we draw a connection between the auxiliary predictive model of the RL system and hippocampus, an area thought to learn a predictive model to support memory-guided behavior. We also connect the encoder network and the value learning network of the RL system to visual cortex and striatum in the brain, respectively. This work demonstrates how representation learning in deep RL systems can provide an interpretable framework for modeling multi-region interactions in the brain. The deep RL perspective taken here also suggests an additional role of the hippocampus in the brain—that of an auxiliary learning system that benefits representation learning in other regions.

1 INTRODUCTION

Deep reinforcement learning (RL) models have shown remarkable success solving challenging problems (Sutton & Barto, 2018; Mnih et al., 2013; Silver et al., 2016; Schulman et al., 2017). These models use neural networks to learn state representations that support complex value functions. A key challenge in this setting is to avoid degenerate representations that support only subpar policies or fail to transfer to related tasks. Self-supervised auxiliary objectives, particularly predictive objectives, have been shown to regularize learning in neural networks to prevent overfit or collapsed representations (Lyle et al., 2021; Dabney et al., 2021; François-Lavet et al., 2019). As such, it is common to combine deep RL objectives with auxiliary objectives. The modular structure of these multi-objective models can function as a metaphor for how different regions of the brain combine to comprise an expressive, generalizable learning system.

Analogy can readily be drawn between the components of a deep RL system augmented with predictive objectives and neural counterparts. For instance, the striatum has been identified as a RL-like value learning system (Schultz et al., 1997). Hippocampus has been linked to learning predictive models and cognitive maps (Mehta et al., 1997; O’Keefe & Nadel, 1978; Koene et al., 2003). Finally, sensory cortex has been suggested to undergo unsupervised or self-supervised learning akin to feature learning (Zhuang et al., 2021), although reward-selective tuning also been observed (Poort et al., 2015). Comparing representations across artificial and biological neural networks can pro-

vide a useful frame of reference for understanding the extent artificial models resemble the brain’s mechanisms for robust and flexible learning.

These comparisons can also provide useful insights into neuroscience, where little is known about how learning in one region might drive representational changes across the brain. For instance, the hippocampus is a likely candidate for predictive objectives, as ample experimental evidence has shown that activity in this region is predictive of the upcoming experience of an animal (Skaggs & McNaughton, 1996; Lisman & Redish, 2009; Mehta et al., 1997; Payne et al., 2021; Muller & Kubie, 1989; Pfeiffer & Foster, 2013; Schapiro et al., 2016; Blum & Abbott, 1996; Mehta et al., 2000). These observations are often accounted for in theoretical work as hippocampus computing a predictive model or map (Lisman & Redish, 2009; Mehta et al., 2000; Russek et al., 2017; Whittington et al., 2020; Momennejad, 2020; George et al., 2021; Stachenfeld et al., 2017). Much has been written about how learned predictive models may be used by the brain to simulate different outcomes or support planning (Vikbladh et al., 2019; Geerts et al., 2020; Mattar & Daw, 2018; Miller et al., 2017; Ólafsdóttir et al., 2018; Redish, 2016; Koene et al., 2003; Foster & Knierim, 2012; McNamee et al., 2021). However, in the context of deep RL, the mere act of learning to make predictions in one region confers substantial benefits to other interconnected regions by shaping representations to incorporate predictive information (Hamrick et al., 2020; Oord et al., 2018; Bengio, 2012). One of the key insights of this work is to propose that an additional role of predictive learning in hippocampus is to drive representation learning that supports deep RL in the brain.

The primary contribution of this paper is to quantify how representations in a deep RL model change with predictive auxiliary objectives, and to identify how these changes mimic representational changes in the brain. We first characterize key functional benefits this auxiliary system confers on learning. We evaluate the effects of predictive auxiliary objectives in a simple gridworld foraging task, and confirm that these objectives help prevent representational collapse, particularly in resource-limited networks. We also observe that longer-horizon predictive objectives are more useful than shorter ones for transfer learning, explaining why novel environments activate longer timescale regions of hippocampus (Fredes et al., 2021). We further demonstrate that a deep RL model with predictive auxiliary objectives undergo a variety of representational phenomena also observed in neural populations in the brain. Downstream objectives can alter activity in the encoder, which is mirrored in various results that show how visual cortical activity is altered by different types of learning. Learning in the prediction module drives activity patterns consistent with activity measured in hippocampus. Overall we find that these interacting objectives explain diverse effects in the neural data not well modeled by considering learning systems in isolation. Moreover, it suggests that deep RL augmented with predictive objectives appears to in many ways mirror the brain’s approach to learning.

2 RELATED WORK

In deep RL, auxiliary objectives have emerged as a crucial tool for representation learning. These additional objectives require internal representations to support other learning goals besides the primary task of value learning. Auxiliary objectives thus regularize internal representations to preserve information that may be relevant for learning. They are thought to address challenges that may arise in sparse reward environments, such as representation collapse and value overfitting (Lyle et al., 2021). Many auxiliary objectives used in machine learning are predictive in flavor. Prior work has found success in defining objectives to predict reward (Jaderberg et al., 2016; Shelhamer et al., 2016) or to predict future states (Shelhamer et al., 2016; Oord et al., 2018; Wayne et al., 2018) from history. Predictive objectives may be useful for additional functions as well. Intrinsic rewards based on the agent’s ability to predict the next state can be used to guide curiosity-driven exploration (Pathak et al., 2017; Tao et al., 2020). These objectives may also aid with transfer learning (Walker et al., 2023), by learning representations that capture features that generalize across diverse domains. The incorporation of auxiliary objectives has greatly enhanced the efficiency and robustness of deep RL models in machine learning applications.

In neuroscience, much theoretical work has sought to characterize brain regions by the computational objective they may be responsible for. Hippocampus in particular has been suggested to learn predictions of an animal’s upcoming experience. This has been formalized as learning a transition model similar to model-based reinforcement learning (Fang et al., 2022) to learning long-horizon

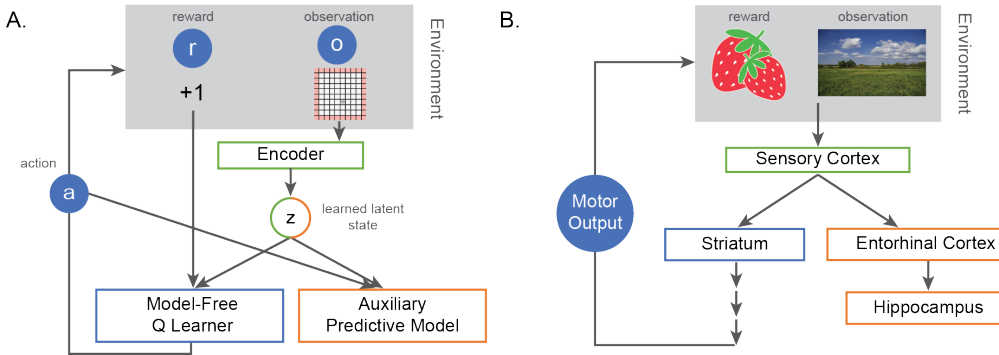


Figure 1: A deep reinforcement learning framework to model the effects of multi-region computation. **A.** Schematic of the deep RL model we use. Reward is provided as a scalar input r . Observations o are 2D visual inputs fed into an encoder (green) that learns low-dimensional state space representations z . The encoder is a convolutional neural network. Representations z are used to learn Q values via a 2-layer MLP (blue); these Q values are used to select actions a . An additional predictive auxiliary objective (orange) is enforced by a separate 2-layer MLP learning predictions from z . **B.** Systems in the brain that are analogous to the encoder, model-free value learning system, and predictive auxiliary task described in (A). A more anatomically accurate and detailed diagram can be found in Appendix Fig A.1.

predictions as in the successor representation (Gershman et al., 2012; Stachenfeld et al., 2017). Separately, the striatum has long been suggested to support model-free (MF) reinforcement learning like actor-critic models (Joel et al., 2002), with more recent work connecting these hypotheses to deep RL settings (Dabney et al., 2021; Lindsey & Litwin-Kumar, 2022).

Less work has been done to understand how the computational objectives of multiple brain regions interact, although this has been suggested as a framework for neuroscience (Marblestone et al., 2016; Yamins & DiCarlo, 2016; Botvinick et al., 2020). Within this literature, a number of groups use multi-region recurrent neural networks (Pinto et al., 2019; Andalman et al., 2019; Kleinman et al., 2021) or switching nonlinear dynamical systems (Semedo et al., 2014; Glaser et al., 2020; Karniol-Tambour et al., 2022) to model the interactions of different regions. However, much of this work focuses more on fitting recorded neural activity than taking a normative perspective on brain function. Some work has sought to construct multi-region models based off computational principles expected in different brain regions (Frank & Claus, 2006; O'Reilly & Frank, 2006; Geerts et al., 2020). Overall, though, the work in this area remains sparse.

In this paper, we establish connections between these two traditions of work in machine learning and neuroscience, in particular showing how deep RL networks can be a multi-region model for neuroscience.

3 EXPERIMENTAL METHODS

Network architecture We implement a double deep Q-learning network (Van Hasselt et al., 2016) with a predictive auxiliary objective, similar to François-Lavet et al. (2019) (Fig 1A). A deep convolutional neural network E encodes observation o_t at time t into a latent state z_t (o_t will be a 2D image depicting the agent state in a tabular grid world in our experiments). The state z_t is used by two network heads: a Q-learning network $Q(z, a)$ that will be used to select action a_t and a prediction network $T(z, a)$ that predicts future latent states. Both Q and T are multi-layer perceptrons with one hidden layer.

Network training procedure The agent is trained on transitions $(o_t, a_t, o_{t+1}, a_{t+1})$ sampled from a random replay buffer. We will also let o_i and o_j denote any two observations randomly sampled from the replay buffer that may not have occurred in sequence.

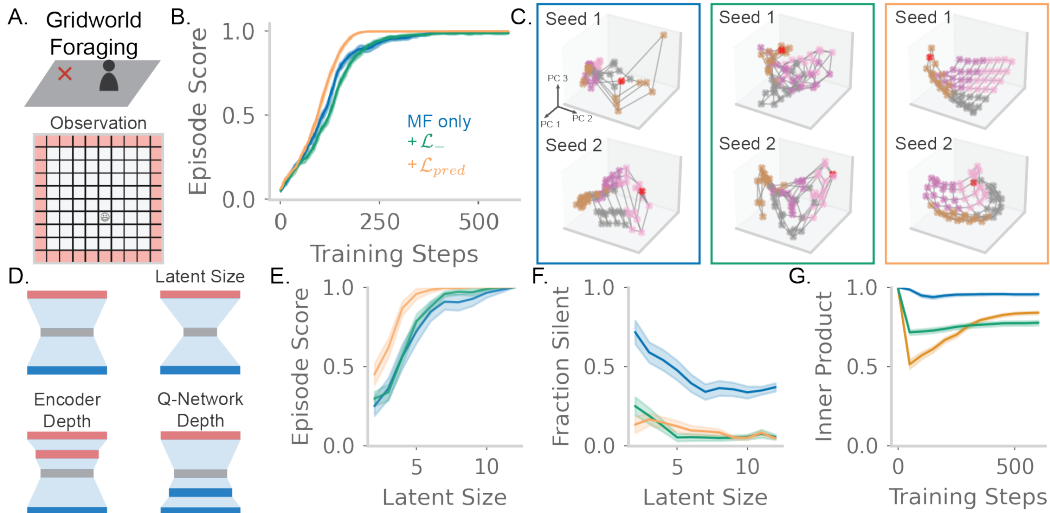


Figure 2: Gridworld performance with predictive auxiliary tasks. **A.** The model is tested on gridworld task in a 8x8 arena. The agent must navigate to a hidden reward given random initial starting locations. **B.** Average episode score across training steps for models without auxiliary losses (blue), with only the negative sampling loss \mathcal{L}_- (green), and with the full predictive loss \mathcal{L}_{pred} (orange). The maximum score is 1 and $|z| = 10$ (i.e. z contains 10 units). Each training step is one batch of replayed transitions that the network is trained on, where the batch size is 64. All error bars are standard error mean over 45 random seeds. **C.** 3D PCA representations of latent states z for the models in (B) (two random seeds). The latent states are colored by the quadrant of the arena they lie in. The quadrants (in order) are purple, pink, gray, brown. The goal location state is colored red. Gray lines represent the true connectivity between states. **D.** We vary $|z|$ (see E, F), as well as the encoder/decoder depths (see Appendix A.2BC). **E.** Average episode score at the end of learning (600 training steps) across $|z|$. **F.** Fraction of units in z that are silent during the task, across $|z|$. **G.** Cosine similarity of two randomly sampled states throughout learning, $|z| = 10$.

The weights of E , Q , T are trained end-to-end to minimize the standard double deep Q-learning temporal difference loss function \mathcal{L}_Q and a predictive auxiliary loss \mathcal{L}_{pred} . The predictive auxiliary loss is similar to that of contrastive predictive coding (Oord et al., 2018). That is, $\mathcal{L}_{pred} = \mathcal{L}_+ + \mathcal{L}_-$ where \mathcal{L}_+ is a positive sampling loss and \mathcal{L}_- is a negative sampling loss.

The positive sample loss is defined as $\mathcal{L}_+ = \|\tau(z_t, a_t) - z_{t+1} - \gamma \tau(o_{t+1}, a_{t+1})\|^2$, where $z_t = E(o_t)$ and $\tau(z_t, a_t) = z_t + T(z_t, a_t)$. This encourages learning of transition-based structure in the encoded representations. Additionally, γ modulates the predictive horizon.

The negative sample loss is defined as $\mathcal{L}_- = -\exp \|\tau(z_i) - z_j\|$. This loss drives temporally distant observations to be represented differently, thereby preventing the trivial solution from being learned (map all latent states to a single point). However, we note that negative sampling elements are not always needed to support self-predictive learning if certain conditions are satisfied (Tang et al., 2023). Except where indicated, the agent learns off-policy via a random policy during learning, only using its policy during test time. The weights over loss terms \mathcal{L}_Q , \mathcal{L}_+ , \mathcal{L}_- are chosen through a small grid search over the final episode score.

Experimental comparisons and modifications We will treat the encoder network as a sensory cortex analog, the Q-learning network as a striatum analog, and the prediction network as a hippocampus analog (Fig 1B). In our analyses, we vary several parameters of interest. We vary the size of z to test the effects of the information bottleneck of the encoder. We will also modulate the strength of γ in the auxiliary loss to test the effects of different timescales of prediction. Finally, we also test how the depths of the decoder and encoder networks affect learning.

4 RESULTS

4.1 PREDICTIVE OBJECTIVES HELP PREVENT REPRESENTATIONAL COLLAPSE.

We first want to understand the effect predictive auxiliary objectives have on a learning system. We test the RL model in a simple gridworld foraging task, where an agent must navigate to a hidden reward from any point in a 2D arena. The observation received by the agent is a 2D image depicting a birds-eye view of the agent’s location. We compare a model without auxiliary objectives (MF-only) to models with the negative sampling objective \mathcal{L}_- only and with the full predictive objective \mathcal{L}_{pred} . Here, the predictive model is trained with one-step prediction ($\gamma = 0$).

Given sufficient capacity in the encoder, decoder, and latent layer z , all models unsurprisingly learn the foraging task (Fig 2B). However, the model with prediction reaches maximum performance with fewer training steps than the both the negative-sampling model and the MF-only agent (Fig 2B). Additionally, the latent representation in the predictive model appears to capture the global structure of the environment better than the other two models (Fig 2C). The model without any auxiliary tasks tends to expand the representation space around rewarding states, while the model with negative sampling (Fig 2C) evenly spaces apart state representations without regard for environment structure.

We next tested how the effects of auxiliary tasks change with the size of the model components (Fig 2D). We first varied the size of z , and thus the representational capacity of the encoder. We find that, although all models can perform well given a large enough latent dimension $|z|$, supplying the model with a predictive auxiliary objective allows the model to learn the task even with a smaller bottleneck (Fig 2E). This benefit is not conveyed by the negative sampling loss alone, suggesting that learning the environment structure confers its own unique benefit (Fig 2E). We find similar results by varying the encoder network depth and the decoder network depth (SuppFig 2), showing that the benefits of predictive auxiliary objectives are more salient in resource-limited cases.

This difference may be because representational collapse is a greater danger in lower-dimensional settings. To test this, we measure how many units in the output of the encoder are involved in supporting the state representation. We find that a greater proportion of units are completely silent in the MF-only encoder (Fig 2F), suggesting a less distributed representation. To more directly test for collapse, we measure how the cosine similarity between state representations change across learning. Although all models start with highly similar states, the models with auxiliary losses separate state representations across training more than the MF-only model does (Fig 2G).

4.2 LONG-HORIZON PREDICTIVE AUXILIARY TASKS ARE MORE EFFECTIVE AT SUPPORTING REPRESENTATIONAL TRANSFER THAN SHORT-HORIZON PREDICTIVE TASKS.

Thus far, we have tested the predictive auxiliary objective with a one-step prediction is used. However, longer horizon predictions are often used as predictive auxiliary objectives (Oord et al., 2018; Hansen et al., 2019), and many neural systems, including hippocampus, have been hypothesized to perform long-horizon predictions (Brunec & Momennejad, 2022; Lee et al., 2021). We next sought to understand under what conditions longer horizons of prediction in auxiliary objectives would be useful. In particular, we were interested in exploring how well learned representations could transfer to new tasks. We hypothesize that long-horizon predictions (larger γ in \mathcal{L}_+) can better capture global environment structure and thus learn representations that transfer better to tasks in similar environments.

We first test representation transfer to new reward locations in gridworld (Fig 3A). After the agent learns an initial goal location in task A, we freeze the encoder, move the goal to a new state, and fine-tune the value network for task B. This allows us to test how well the learned representation structure can support new value functions. We test models with \mathcal{L}_{pred} loss and $\gamma \in \{0.0, 0.25, 0.5, 0.8\}$. We find that, although all models learn task A quickly, models with larger γ learn task B more efficiently (Fig 3B). We test how this effect scales with latent sizes. Just having a predictive horizon longer than one timestep appears sufficient to improve learning efficiency, with the effect stronger at larger latent sizes. (Fig 3C). The selective benefit of longer time horizons for transfer may explain the observation that regions of hippocampus with larger spatial scales appear to be preferentially active in novel environments (Fredes et al., 2021; Köhler et al., 2002; Poppenk et al., 2010).

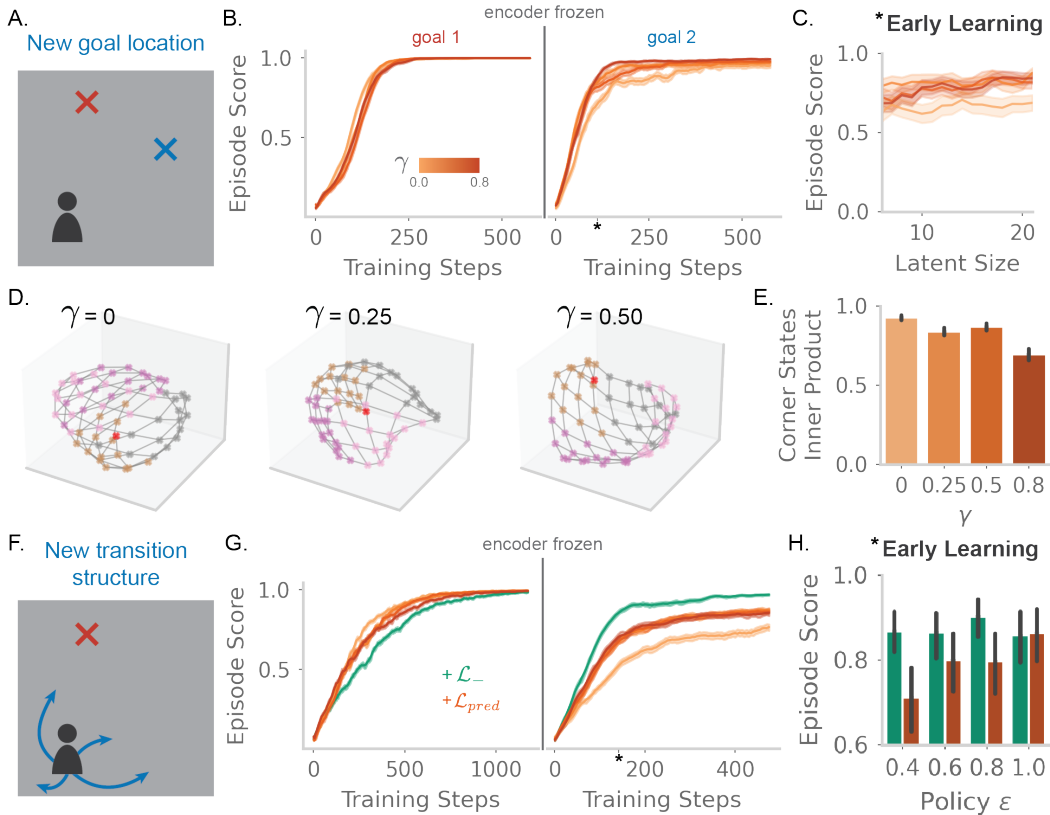


Figure 3: Effects of predictive auxiliary objectives across transfer learning scenarios. **A.** We test goal transfer by moving the goal location to a new state in task B. After training on task A, encoder weights are frozen and the value function is fine-tuned on task B. **B.** Average episode score across task A, then task B. All models shown use the predictive auxiliary loss, with the shade of each line corresponding to the magnitude of γ in \mathcal{L}_{pred} ($\gamma \in \{0.0, 0.25, 0.5, 0.8\}$, $|z| = 17$). **C.** The episode score after 100 training steps for each of the models in (B), as $|z|$ is increased. All models achieve maximum performance in task A. 30 random seeds are run for each latent size. **D.** 3D PCA plots, for three models ($\gamma = 0.0, 0.25, 0.5$) with the same random seed. **E.** Pairwise cosine similarity values between the corner states of the arena for the model shown in (B). **F.** We test transition transfer by shuffling the connectivity between all states in task B. Freezing and fine-tuning are the same as in (A). **G.** Average episode score across task A, then task B. Here, $|z| = 17$ and $\epsilon = 0.4$ -greedy policy during learning. In green is the model with only \mathcal{L}_- as an auxiliary loss. **H.** Episode score after 150 training steps for the model with only \mathcal{L}_- (green) versus the model with \mathcal{L}_{pred} for $\gamma = 0.8$. On the x-axis, the policy ϵ used during training is varied, with $\epsilon = 1.0$ corresponding to a fully random policy ($|z| = 17$, all models have achieved maximum performance on task A).

We hypothesize that the difference in efficient transfer performance across the models may result from learning a latent structure that better reflects global structure. Long-horizon prediction may be better at smoothing across experience over many timesteps, thus capturing global environment structure better than short-horizon prediction and providing a larger benefit when latent representations are higher dimensional. Indeed, models with smaller γ values tend to learn more curved maps that preserve local, but not global, structure (Fig 3D). To quantify this effect, we measured the inner product between the states representing the corners of the environment. These are states that are maximally far from each other, and as such, representations that capture the environment structure accurately should separate these states from each other. We see that, across learning, models with larger γ learn to separate corner states better (Fig 3E).

Predictive auxiliary objectives can also be disadvantageous under certain regimes. Under predictive objectives, latent representations are shaped to reflect transition structure. However, these learned

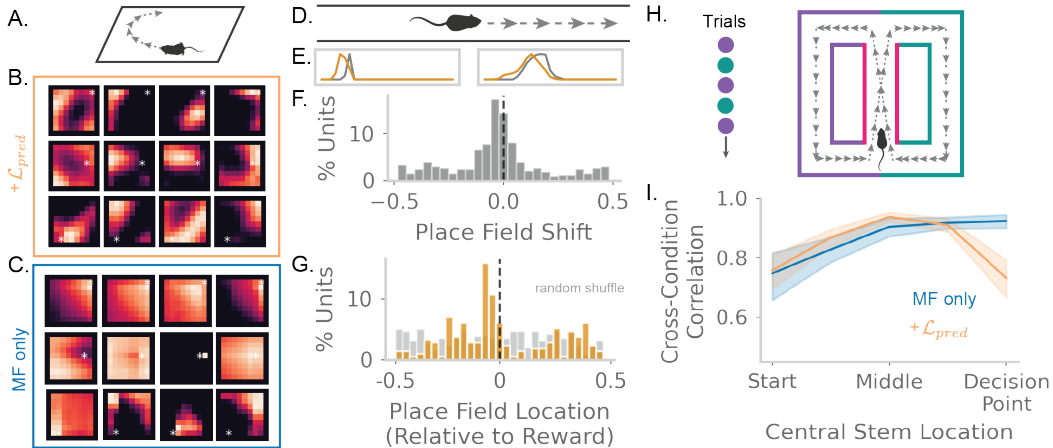


Figure 4: Representational changes in the predictive model are similar to those observed in the hippocampus. **A.** 2D foraging experiments are simulated as in the gridworld task from Fig 1-2. **B.** 2D receptive fields from top four T units (columns) sorted by spatial information score (Skaggs et al., 1992). Three random seeds are shown (rows). The model uses \mathcal{L}_{pred} and $|z| = 10$. White asterisk depicts reward. **C.** As in (B), but the model has no auxiliary objectives. **D.** We simulate circular track experiments using a circular gridworld environment with 28 states. The agent receives reward by running laps in a clockwise fashion, with reward in a random state for each random seed. **E.** Receptive fields of two example units in the T network before learning (gray) and after learning (orange). **F.** Histogram over the shift in receptive field peaks for individual units in T over 15 random seeds, where $|z| = 24$. Positive shift values are in the forward movement direction, and vice-versa for negative shift values. Black dotted line at 0. Median of the histogram is -0.034 . **G.** Histogram over the location of receptive field peaks for units in (F), with location centered around the reward site. Random shuffle (gray) control was made by randomly shuffling the weights of the T network. Black dotted line at 0. The model median is -0.06 , while the random shuffle median is -0.02 . **H.** We simulate a 5×5 alternating-T maze (details in Appendix). Center corridor is colored pink. **I.** Cosine similarity of T population vector responses in the center corridor under left-turn versus right-turn conditions. X-axis depicts location in the center corridor. Data is from 20 random seeds. Shown is the model without auxiliary objectives (blue) and the model with \mathcal{L}_{pred} (orange). T is randomly initialized for the model without an auxiliary objective.

representations might not generalize well to new tasks where the transition structure or the policy changes. We test this in a different transfer task, where reward location remains the same in task B, but the environment transition structure is scrambled (Fig 3F). Additionally, to test for effects of policy change across task A and B, we vary the portion of random actions taken in our ϵ -greedy agent. Under this new transfer task with $\epsilon = 0.4$, we find a marked decrease in task B performance for models with the predictive objective compared to a model with just the negative sampling loss. (Fig. 3G).

Indeed, as ϵ gets smaller and the agent learns more from biased on-policy transition statistics, transfer performance on task B accordingly suffers (Fig 3G,H). All models with predictive objectives do not perform as well in task B as a model with only negative sampling loss (Fig 3G,H).

4.3 EFFECTS OF VALUE LEARNING AND HISTORY-DEPENDENCE IN PREDICTION NETWORK RESEMBLE HIPPOCAMPAL ACTIVITY.

We next ask how well representations developed in the network can model representations found in neural activity. The output of our T network serves as an analog to the hippocampus, a region implicated in self-predictive learning. We first test whether the T network activity can capture a classic result in the hippocampal literature: formation of spatially local activity patterns, called place fields. We plot the spatial firing fields of individual T units in our model trained on gridworld,

and find 2D place fields as expected (Fig 4B). We also find that the prevalence of these place fields is greatly reduced in models without predictive auxiliary tasks (Fig 4C).

Hippocampal place fields also undergo to experience-dependent changes. We test for these effects in our model through 1D circular track experiments (Fig 4D). We find that place fields developed on the 1D track will skew and shift backwards from the movement of the animal (Fig 4E,F). This is consistent with phenomena in rodent hippocampal data that have been attributed to predictive learning (Mehta et al., 2000). We also find that the number of place fields across the linear track is more abundant close to the reward site (Fig 4G), another widely observed phenomena that is considered to be a result of reward learning in hippocampus. Our results suggest that value learning in shared representations with other systems can result in reward-related effects in the hippocampus.

Finally, we test a more complex form of experience-dependency in neural activity by simulating an alternating T-maze task. In this task, animals are required to alternate between two trial types: one where they run down a center corridor and turn left for reward, and another where they run down the same center corridor but turn right for reward. In these tasks, neural activity has been observed to “split” – that is, neurons fire differently in the center corridor across trial types despite the spatial details of the corridor remaining the same (Duvelle et al., 2023). Interestingly, the degree of splitting is greatest in the beginning of the corridor and also high at the end of the corridor, splitting least in the middle of the corridor (Duvelle et al., 2023). To enable the agent to perform this task, which requires remembering whether the previous trial type, we introduce a memory component to the agent so that a temporally graded trace of previous observations are made available (?). We measure cosine similarity between population activity in the left turn condition and the right turn condition. Lower similarity corresponds to greater splitting. The representations in both a MF-only model and the model with the predictive objective show increased splitting in the beginning of the corridor due to the memory component (Fig 4F). However, only the model with the predictive objective shows increased splitting at the end of the corridor (Fig 4F). This shows that the pattern of splitting seen in data can be captured by a model using both memory and prediction.

4.4 EFFECTS OF VALUE LEARNING AND TRANSITION LEARNING IN THE ENCODER NETWORK RESEMBLE ACTIVITY IN VISUAL CORTEX.

As another example of representational effects arising from mutually interacting regions, we compare the activity of our encoder network to experimental results in sensory cortices. Neurons in visual cortex (even those in primary regions) have been observed to change their tuning as a result of learning Poort et al. (2015); Li & DiCarlo (2008; 2010); Wilmes & Clopath (2019); Pakan et al. (2018). Our model provides a simple system to look for such effects.

First, we test for effects of prediction and temporal statistics that have been seen in visual cortex. Specifically, Li & DiCarlo (2008) found that object selectivity in macaque IT neurons could be altered by exposing animals to sequences of images where preferred stimuli and non-preferred stimuli became linked (Fig 5A). The images in the preferred and non-preferred that are linked together are referred to as the “swap position” within a sequence (Fig 5A). An analogous experiment can be run in our gridworld task from Fig 2. We first identify spatially contiguous preferred and non-preferred states of neurons in the encoder network. We then expose the model to sequences where preferred states and non-preferred states became connected at arbitrarily chosen swap positions (Fig 5B). We find neurons in the output of the encoder that, after exposure, decrease their firing rate for the preferred stimulus at the swap location and increase their firing rate for the non-preferred stimulus at the swap position (Fig 5C). This is consistent with observations in data as well (Li & DiCarlo, 2008; 2010). We quantify this change in firing rate at different sequence locations. We find a similar trend as in data, where tuning for stimuli closer to the swap position is increasingly altered away from the original preferences (Fig 5D). Importantly, this effect is not present without the predictive auxiliary objective, similar to lesion studies carried out in Finnie et al. (2021).

The downstream Q-learning objective also have an effect on representations in the encoder. We simulate value learning effects in visual cortical activity through linear track experiments used in Poort et al. (2015) (Fig 5E). In this experiment, authors found that V1 neurons in mice increased selectivity for visual cues in the environment after learning the task. Furthermore, the authors noted a slight selectivity increase for more rewarding cues (vertical gratings) compared to nonrewarding cues (angled gratings). We find a similar effect in units in early layers of the encoder network: a

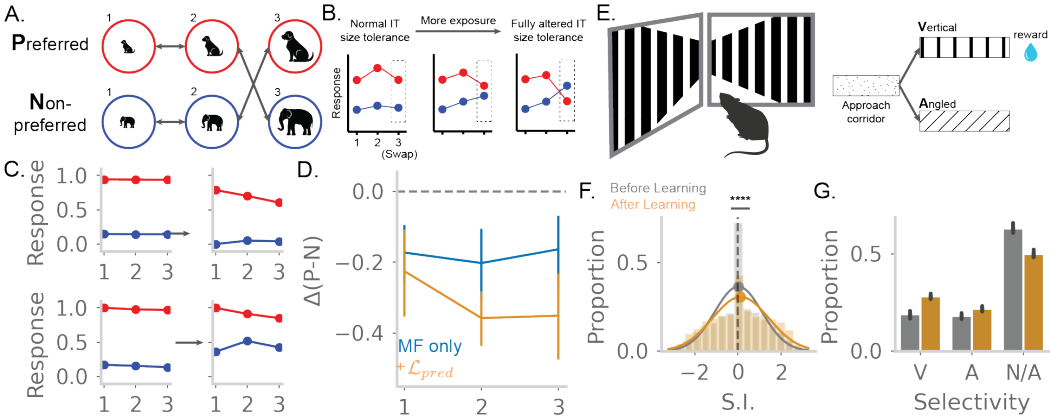


Figure 5: Representational changes in the encoder model resemble recordings from visual cortex. **A.** Example of the sequence structure in the preference swap task of Li & DiCarlo (2008; 2010), with images numbered by their location in the sequence. **B.** Reproduced schematic from Li & DiCarlo (2010) of the changes in IT neuron response to preferred images (red) and non-preferred images (blue) across exposure to new image transitions. **C.** Responses of two example units from the model with \mathcal{L}_{pred} . Arrows indicate response profile before and after experiencing swapped transitions. Red indicates the response to $P1, P2, P3$ states that were selected from the gridworld environment, while blue indicates the response to $N1, N2, N3$ states selected from the environment. **D.** Change in response difference between $(P1, N1)$, $(P2, N2)$, and $(P3, N3)$ over 10 units. Each unit is a separate transition swap experiment. Shown is the model without any auxiliary objectives (blue) and the model with \mathcal{L}_{pred} (orange). **E.** Linear track VR experiment used in Poort et al. (2015). Vertical stripe corridors led to reward, while angled corridors did not lead to any consequence. Animals experienced either condition at random following an approach corridor with random noise stimuli. **F.** Selectivity across the population before learning (gray) and after learning (orange). Selectivity was calculated as in Poort et al. (2015), with negative and positive values corresponding to angled and vertical corridor preference, respectively. Asterisks indicate significance from one-tailed Welch's t-test (t-statistic: -12.43 , p-value: 9×10^{-36}). **G.** Selectivity of individual units before (gray) and after (orange) learning for vertical condition (V), angled condition (A), or neither (N/A). Units are pooled across 15 experiments.

small, but statistically significant increase in proportion of units encoding the rewarded stimulus (Fig 5F). As in Poort et al. (2015), selectivity increases across learning, but with a greater preference for the vertical grating environment (Fig 5G).

5 CONCLUSION

In this work, we explore the representational effects induced by predictive auxiliary objectives. We show how such objectives are useful in resource-limited settings and in certain transfer learning settings. We also investigate how prediction and predictive horizons affect learned representation structure. Furthermore, we describe how such deep RL models can function as a multi-region model for neuroscience. We show how representation learning in the prediction model recapitulates experimental observations made in the hippocampus. We make similar connections between representation learning in the encoder model and learning in visual cortex.

Our results point to a new perspective on the role of the hippocampus in learning. That is, a predictive system like the hippocampus can be useful for learning without being used to generate sequences or support planning. Learning predictions is sufficient to induce useful structure into representations used by other regions. This view also connects to trends seen in machine learning literature. In deep RL, predictive models need not be used for forward planning (Hamrick et al., 2020) to be useful for representation learning. Additionally, the contrastive prediction objective used in this work is drawn from machine learning literature but bears interesting similarities to classic descriptions of hippocampal computation. CA3 and CA1 in the hippocampus have been implicated in predictive

learning similar to the positive sampling loss. Meanwhile, the dentate gyrus in the hippocampus has been proposed to perform pattern separation similar to the contrastive negative sampling loss.

Overall, this work points to the utility of a modeling approach that considers the effect of multiple objectives in a deep learning system. The deep network setting reveals new aspects of neuroscience modeling that are less apparent in tabular settings or in simpler models.

REFERENCES

Aaron S Andalman, Vanessa M Burns, Matthew Lovett-Barron, Michael Broxton, Ben Poole, Samuel J Yang, Logan Grosenick, Talia N Lerner, Ritchie Chen, Tyler Benster, et al. Neuronal dynamics regulating brain and behavioral state transitions. *Cell*, 177(4):970–985, 2019.

Yoshua Bengio. Deep learning of representations for unsupervised and transfer learning. In *Proceedings of ICML workshop on unsupervised and transfer learning*, pp. 17–36. JMLR Workshop and Conference Proceedings, 2012.

Kenneth I Blum and Larry F Abbott. A model of spatial map formation in the hippocampus of the rat. *Neural computation*, 8(1):85–93, 1996.

Matthew Botvinick, Jane X Wang, Will Dabney, Kevin J Miller, and Zeb Kurth-Nelson. Deep reinforcement learning and its neuroscientific implications. *Neuron*, 107(4):603–616, 2020.

Iva K. Brunec and Ida Momennejad. Predictive representations in hippocampal and prefrontal hierarchies. *Journal of Neuroscience*, 42(2):299–312, 2022. ISSN 0270-6474. doi: 10.1523/JNEUROSCI.1327-21.2021. URL <https://www.jneurosci.org/content/42/2/299>.

Cathrin B Canto, Floris G Wouterlood, Menno P Witter, et al. What does the anatomical organization of the entorhinal cortex tell us? *Neural plasticity*, 2008, 2008.

Will Dabney, André Barreto, Mark Rowland, Robert Dadashi, John Quan, Marc G Bellemare, and David Silver. The value-improvement path: Towards better representations for reinforcement learning. In *Proceedings of the AAAI Conference on Artificial Intelligence*, volume 35, pp. 7160–7168, 2021.

Éléonore Duvelle, Roddy M Grieves, and Matthijs AA van der Meer. Temporal context and latent state inference in the hippocampal splitter signal. *Elife*, 12:e82357, 2023.

Ching Fang, Dmitriy Aronov, Larry F Abbott, and Emily Mackevicius. Neural learning rules for generating flexible predictions and computing the successor representation. *bioRxiv*, pp. 2022–05, 2022.

Peter SB Finnie, Robert W Komorowski, and Mark F Bear. The spatiotemporal organization of experience dictates hippocampal involvement in primary visual cortical plasticity. *Current Biology*, 31(18):3996–4008, 2021.

David J Foster and James J Knierim. Sequence learning and the role of the hippocampus in rodent navigation. *Current opinion in neurobiology*, 22(2):294–300, 2012.

Vincent François-Lavet, Yoshua Bengio, Doina Precup, and Joelle Pineau. Combined reinforcement learning via abstract representations. In *Proceedings of the AAAI Conference on Artificial Intelligence*, volume 33, pp. 3582–3589, 2019.

Michael J Frank and Eric D Claus. Anatomy of a decision: striato-orbitofrontal interactions in reinforcement learning, decision making, and reversal. *Psychological review*, 113(2):300, 2006.

Felipe Fredes, Maria Alejandra Silva, Peter Koppensteiner, Kenta Kobayashi, Maximilian Joesch, and Ryuichi Shigemoto. Ventro-dorsal hippocampal pathway gates novelty-induced contextual memory formation. *Current Biology*, 31(1):25–38.e5, 2021. ISSN 0960-9822. doi: <https://doi.org/10.1016/j.cub.2020.09.074>. URL <https://www.sciencedirect.com/science/article/pii/S0960982220314445>.

Jesse P Geerts, Fabian Chersi, Kimberly L Stachenfeld, and Neil Burgess. A general model of hippocampal and dorsal striatal learning and decision making. *Proceedings of the National Academy of Sciences*, 117(49):31427–31437, 2020.

Dileep George, Rajeev V Rikhye, Nishad Gothoskar, J Swaroop Guntupalli, Antoine Dedieu, and Miguel Lázaro-Gredilla. Clone-structured graph representations enable flexible learning and vicarious evaluation of cognitive maps. *Nature communications*, 12(1):1–17, 2021.

Samuel J Gershman, Christopher D Moore, Michael T Todd, Kenneth A Norman, and Per B Sederberg. The successor representation and temporal context. *Neural Computation*, 24(6):1553–1568, 2012.

Joshua Glaser, Matthew Whiteway, John P Cunningham, Liam Paninski, and Scott Linderman. Recurrent switching dynamical systems models for multiple interacting neural populations. *Advances in neural information processing systems*, 33:14867–14878, 2020.

Sarah C Goodroe, Jon Starnes, and Thackery I Brown. The complex nature of hippocampal-striatal interactions in spatial navigation. *Frontiers in human neuroscience*, 12:250, 2018.

Jessica B Hamrick, Abram L Friesen, Feryal Behbahani, Arthur Guez, Fabio Viola, Sims Witherpoon, Thomas Anthony, Lars Buesing, Petar Veličković, and Théophane Weber. On the role of planning in model-based deep reinforcement learning. *arXiv preprint arXiv:2011.04021*, 2020.

Steven Hansen, Will Dabney, André Barreto, Tom Van de Wiele, David Warde-Farley, and Volodymyr Mnih. Fast task inference with variational intrinsic successor features. *CoRR*, abs/1906.05030, 2019. URL <http://arxiv.org/abs/1906.05030>.

Max Jaderberg, Volodymyr Mnih, Wojciech Marian Czarnecki, Tom Schaul, Joel Z Leibo, David Silver, and Koray Kavukcuoglu. Reinforcement learning with unsupervised auxiliary tasks. *arXiv preprint arXiv:1611.05397*, 2016.

Daphna Joel, Yael Niv, and Eytan Ruppin. Actor-critic models of the basal ganglia: New anatomical and computational perspectives. *Neural networks*, 15(4-6):535–547, 2002.

Orren Karniol-Tambour, David M Zoltowski, E Mika Diamanti, Lucas Pinto, David W Tank, Carlos W Brody, and Jonathan W Pillow. Modeling communication and switching nonlinear dynamics in multi-region neural activity. *bioRxiv*, pp. 2022–09, 2022.

Michael Kleinman, Chandramouli Chandrasekaran, and Jonathan Kao. A mechanistic multi-area recurrent network model of decision-making. *Advances in neural information processing systems*, 34:23152–23165, 2021.

Randal A Koene, Anatoli Gorchetchnikov, Robert C Cannon, and Michael E Hasselmo. Modeling goal-directed spatial navigation in the rat based on physiological data from the hippocampal formation. *Neural Networks*, 16(5-6):577–584, 2003.

Stefan Köhler, Joelle Crane, and Brenda Milner. Differential contributions of the parahippocampal place area and the anterior hippocampus to human memory for scenes. *Hippocampus*, 12(6):718–723, 2002.

Caroline S Lee, Mariam Aly, and Christopher Baldassano. Anticipation of temporally structured events in the brain. *eLife*, 10:e64972, apr 2021. ISSN 2050-084X. doi: 10.7554/eLife.64972. URL <https://doi.org/10.7554/eLife.64972>.

Nuo Li and James J DiCarlo. Unsupervised natural experience rapidly alters invariant object representation in visual cortex. *science*, 321(5895):1502–1507, 2008.

Nuo Li and James J DiCarlo. Unsupervised natural visual experience rapidly reshapes size-invariant object representation in inferior temporal cortex. *Neuron*, 67(6):1062–1075, 2010.

Jack Lindsey and Ashok Litwin-Kumar. Action-modulated midbrain dopamine activity arises from distributed control policies. *Advances in Neural Information Processing Systems*, 35:5535–5548, 2022.

John Lisman and A David Redish. Prediction, sequences and the hippocampus. *Philosophical Transactions of the Royal Society B: Biological Sciences*, 364(1521):1193–1201, 2009.

Clare Lyle, Mark Rowland, Georg Ostrovski, and Will Dabney. On the effect of auxiliary tasks on representation dynamics. In *International Conference on Artificial Intelligence and Statistics*, pp. 1–9. PMLR, 2021.

Adam H Marblestone, Greg Wayne, and Konrad P Kording. Toward an integration of deep learning and neuroscience. *Frontiers in computational neuroscience*, 10:94, 2016.

Marcelo G Mattar and Nathaniel D Daw. Prioritized memory access explains planning and hippocampal replay. *Nature neuroscience*, 21(11):1609–1617, 2018.

Daniel C McNamee, Kimberly L Stachenfeld, Matthew M Botvinick, and Samuel J Gershman. Flexible modulation of sequence generation in the entorhinal-hippocampal system. *Nature neuroscience*, 24(6):851–862, June 2021. ISSN 1097-6256. doi: 10.1038/s41593-021-00831-7. URL <https://europepmc.org/articles/PMC7610914>.

Mayank R Mehta, Carol A Barnes, and Bruce L McNaughton. Experience-dependent, asymmetric expansion of hippocampal place fields. *Proceedings of the National Academy of Sciences*, 94(16):8918–8921, 1997.

Mayank R Mehta, Michael C Quirk, and Matthew A Wilson. Experience-dependent asymmetric shape of hippocampal receptive fields. *Neuron*, 25(3):707–715, 2000.

Kevin J Miller, Matthew M Botvinick, and Carlos D Brody. Dorsal hippocampus contributes to model-based planning. *Nature neuroscience*, 20(9):1269–1276, 2017.

Volodymyr Mnih, Koray Kavukcuoglu, David Silver, Alex Graves, Ioannis Antonoglou, Daan Wierstra, and Martin Riedmiller. Playing atari with deep reinforcement learning. *arXiv preprint arXiv:1312.5602*, 2013.

Ida Momennejad. Learning structures: predictive representations, replay, and generalization. *Current Opinion in Behavioral Sciences*, 32:155–166, 2020.

Nicolás A Morgenstern, Ana Filipa Isidro, Inbal Israely, and Rui M Costa. Pyramidal tract neurons drive amplification of excitatory inputs to striatum through cholinergic interneurons. *Science Advances*, 8(6):eabh4315, 2022.

Robert U. Muller and John L Kubie. The firing of hippocampal place cells predicts the future position of freely moving rats. In *The Journal of neuroscience : the official journal of the Society for Neuroscience*, 1989.

J. O’Keefe and L. Nadel. *The hippocampus as a cognitive map*. Clarendon Press, Oxford, United Kingdom, 1978.

H Freyja Ólafsdóttir, Daniel Bush, and Caswell Barry. The role of hippocampal replay in memory and planning. *Current Biology*, 28(1):R37–R50, 2018.

Aaron van den Oord, Yazhe Li, and Oriol Vinyals. Representation learning with contrastive predictive coding. *arXiv preprint arXiv:1807.03748*, 2018.

Randall C O’Reilly and Michael J Frank. Making working memory work: a computational model of learning in the prefrontal cortex and basal ganglia. *Neural computation*, 18(2):283–328, 2006.

Janelle MP Pakan, Valerio Francioni, and Nathalie L Rochefort. Action and learning shape the activity of neuronal circuits in the visual cortex. *Current opinion in neurobiology*, 52:88–97, 2018.

Deepak Pathak, Pulkit Agrawal, Alexei A Efros, and Trevor Darrell. Curiosity-driven exploration by self-supervised prediction. In *International conference on machine learning*, pp. 2778–2787. PMLR, 2017.

HL Payne, GF Lynch, and D Aronov. Neural representations of space in the hippocampus of a food-caching bird. *Science*, 373(6552):343–348, 2021.

Brad E Pfeiffer and David J Foster. Hippocampal place-cell sequences depict future paths to remembered goals. *Nature*, 497(7447):74–79, 2013.

Lucas Pinto, Kanaka Rajan, Brian DePasquale, Stephan Y Thibierge, David W Tank, and Carlos D Brody. Task-dependent changes in the large-scale dynamics and necessity of cortical regions. *Neuron*, 104(4):810–824, 2019.

Jasper Poort, Adil G Khan, Marius Pachitariu, Abdellatif Nemri, Ivana Orsolic, Julija Krupic, Marius Bauza, Maneesh Sahani, Georg B Keller, Thomas D Mrsic-Flogel, et al. Learning enhances sensory and multiple non-sensory representations in primary visual cortex. *Neuron*, 86(6):1478–1490, 2015.

Jordan Poppenk, Anthony R McIntosh, Fergus IM Craik, and Morris Moscovitch. Past experience modulates the neural mechanisms of episodic memory formation. *Journal of Neuroscience*, 30(13):4707–4716, 2010.

A David Redish. Vicarious trial and error. *Nature Reviews Neuroscience*, 17(3):147–159, 2016.

EM Russek, Momennejad I, MM Botvinick, SJ Gershman, and ND Daw. Predictive representations can link model-based reinforcement learning to model-free mechanisms. *PLoS Comput Biol*, 2017. doi: 10.1371/journal.pcbi.1005768.

Anna C Schapiro, Nicholas B Turk-Browne, Kenneth A Norman, and Matthew M Botvinick. Statistical learning of temporal community structure in the hippocampus. *Hippocampus*, 26(1):3–8, 2016.

John Schulman, Filip Wolski, Prafulla Dhariwal, Alec Radford, and Oleg Klimov. Proximal policy optimization algorithms. *arXiv preprint arXiv:1707.06347*, 2017.

Wolfram Schultz, Peter Dayan, and P Read Montague. A neural substrate of prediction and reward. *Science*, 275(5306):1593–1599, 1997.

Joao Semedo, Amin Zandvakili, Adam Kohn, Christian K Machens, and Byron M Yu. Extracting latent structure from multiple interacting neural populations. *Advances in neural information processing systems*, 27, 2014.

Evan Shelhamer, Parsa Mahmoudieh, Max Argus, and Trevor Darrell. Loss is its own reward: Self-supervision for reinforcement learning. *arXiv preprint arXiv:1612.07307*, 2016.

David Silver, Aja Huang, Chris J Maddison, Arthur Guez, Laurent Sifre, George Van Den Driessche, Julian Schrittwieser, Ioannis Antonoglou, Veda Panneershelvam, Marc Lanctot, et al. Mastering the game of go with deep neural networks and tree search. *nature*, 529(7587):484–489, 2016.

WE Skaggs and BL McNaughton. Replay of neuronal firing sequences in rat hippocampus during sleep following spatial experience. *Science*, 1996. doi: 10.1126/science.271.5257.1870.

William Skaggs, Bruce McNaughton, and Katalin Gothard. An information-theoretic approach to deciphering the hippocampal code. *Advances in neural information processing systems*, 5, 1992.

Kimberly Stachenfeld, Matthew Botvinick, and Samuel Gershman. The hippocampus as a predictive map. *Nature Neuroscience*, 2017. doi: 10.1038/nn.4650.

Richard S Sutton and Andrew G Barto. *Reinforcement learning: An introduction*. MIT press, 2018.

Yunhao Tang, Zhaohan Daniel Guo, Pierre Harvey Richemond, Bernardo Avila Pires, Yash Chandak, Rémi Munos, Mark Rowland, Mohammad Gheshlaghi Azar, Charline Le Lan, Clare Lyle, et al. Understanding self-predictive learning for reinforcement learning. In *International Conference on Machine Learning*, pp. 33632–33656. PMLR, 2023.

Ruo Yu Tao, Vincent François-Lavet, and Joelle Pineau. Novelty search in representational space for sample efficient exploration. *Advances in Neural Information Processing Systems*, 33:8114–8126, 2020.

Hado Van Hasselt, Arthur Guez, and David Silver. Deep reinforcement learning with double q-learning. In *Proceedings of the AAAI conference on artificial intelligence*, volume 30, 2016.

Oliver M Vikbladh, Michael R Meager, John King, Karen Blackmon, Orrin Devinsky, Daphna Shohamy, Neil Burgess, and Nathaniel D Daw. Hippocampal contributions to model-based planning and spatial memory. *Neuron*, 102(3):683–693, 2019.

Jacob C Walker, Eszter Vértes, Yazhe Li, Gabriel Dulac-Arnold, Ankesh Anand, Théophane Weber, and Jessica B Hamrick. Investigating the role of model-based learning in exploration and transfer. In *International Conference on Machine Learning*, pp. 35368–35383. PMLR, 2023.

Greg Wayne, Chia-Chun Hung, David Amos, Mehdi Mirza, Arun Ahuja, Agnieszka Grabska-Barwinska, Jack Rae, Piotr Mirowski, Joel Z Leibo, Adam Santoro, et al. Unsupervised predictive memory in a goal-directed agent. *arXiv preprint arXiv:1803.10760*, 2018.

James CR Whittington, Timothy H Muller, Shirley Mark, Guifen Chen, Caswell Barry, Neil Burgess, and Timothy EJ Behrens. The tolman-eichenbaum machine: Unifying space and relational memory through generalization in the hippocampal formation. *Cell*, 183(5):1249–1263, 2020.

Katharina Anna Wilmes and Claudia Clopath. Inhibitory microcircuits for top-down plasticity of sensory representations. *Nature communications*, 10(1):5055, 2019.

Daniel LK Yamins and James J DiCarlo. Using goal-driven deep learning models to understand sensory cortex. *Nature neuroscience*, 19(3):356–365, 2016.

Chengxu Zhuang, Siming Yan, Aran Nayebi, Martin Schrimpf, Michael C. Frank, James J. DiCarlo, and Daniel L. K. Yamins. Unsupervised neural network models of the ventral visual stream. *Proceedings of the National Academy of Sciences*, 118(3):e2014196118, 2021. doi: 10.1073/pnas.2014196118. URL <https://www.pnas.org/doi/abs/10.1073/pnas.2014196118>.

A APPENDIX

A.1 ALTERNATING-T MAZE SIMULATION

The maze is 5×5 . That is, the agent enters the center stem at $(x = 2, y = 0)$ and reaches the decision point at $(x = 2, y = 4)$. The agent is incentivized to follow a figure-8 path via invisible barriers and the presence of reward at $(0, 4)$, $(2, 4)$, and $(4, 4)$. The model is simulated with a 6-frame memory trace with weight decay of 0.9.

A.2 GRIDSEARCH FOR LEARNING RATES

Weights below are formatted as $[Q \text{ Loss}, \mathcal{L}_-, \mathcal{L}_+]$

- MF Only: $[[1e-5, 0, 0], [1e-4, 0, 0], [1e-3, 0, 0]]$
- MF + Negative Sampling: $[[1e-4, 1e-6, 0], [1e-4, 1e-5, 0], [1e-4, 1e-4, 0], [1e-4, 1e-3, 0], [1e-4, 1e-2, 0]]$
- MF + Positive Sampling, $\gamma = 0$: $[[1e-4, 1e-6, 1e-6], [1e-4, 1e-5, 1e-6], [1e-4, 1e-4, 1e-6], [1e-4, 1e-3, 1e-6]]$
- MF + Positive Sampling, $\gamma = 0.25$: $[[1e-4, 1e-6, 1e-6], [1e-4, 1e-5, 1e-6], [1e-4, 1e-4, 1e-6], [1e-4, 1e-3, 1e-6], [1e-4, 1e-6, 1e-7], [1e-4, 1e-5, 1e-7], [1e-4, 1e-4, 1e-7], [1e-4, 1e-3, 1e-7]]$
- MF + Positive Sampling, $\gamma = 0.5$: $[[1e-4, 1e-6, 1e-6], [1e-4, 1e-5, 1e-6], [1e-4, 1e-4, 1e-6], [1e-4, 1e-3, 1e-6], [1e-4, 1e-6, 1e-7], [1e-4, 1e-5, 1e-7], [1e-4, 1e-4, 1e-7], [1e-4, 1e-3, 1e-7]]$
- MF + Positive Sampling, $\gamma = 0.8$: $[[1e-4, 1e-6, 1e-7], [1e-4, 1e-5, 1e-7], [1e-4, 1e-4, 1e-7], [1e-4, 1e-3, 1e-7], [1e-4, 1e-6, 1e-8], [1e-4, 1e-5, 1e-7], [1e-4, 1e-4, 1e-8], [1e-4, 1e-3, 1e-8]]$

A.3 PARAMETERS FOR BASE NETWORK

Module	Layer	Activation
Encoder Network	Conv2D: 16 channels, 2x2 kernel size	ReLU
	Conv2D: 32 channels, 2x2 kernel size	ReLU
	MaxPool2D, 2x2 kernel size	
	Fully Connected: output size 32	ReLU
	Fully Connected: output size $ z $	ReLU
Q Network	Fully Connected: output size 16	ReLU
	Fully Connected: output size 1	
T Network	Fully Connected: output size 16	ReLU
	Fully Connected: output size $ z $	

Table 1: Learning Rates

Model	Q Loss	L_-	L_+
MF Only	$1e-4$	0	0
MF + Negative Sampling	$1e-4$	$1e-4$	0
MF + Negative & Positive Sampling, $\gamma = 0$	$1e-4$	$1e-5$	$1e-6$
MF + Negative & Positive Sampling, $\gamma = 0.25$	$1e-4$	$1e-4$	$1e-6$
MF + Negative & Positive Sampling, $\gamma = 0.5$	$1e-4$	$1e-4$	$1e-7$
MF + Negative & Positive Sampling, $\gamma = 0.8$	$1e-4$	$1e-4$	$1e-8$

A.4 PARAMETERS FOR NETWORK WITH DEEPER ENCODER

Module	Layer	Activation
Encoder Network	Conv2D: 16 channels, 2x2 kernel size	ReLU
	Conv2D: 48 channels, 2x2 kernel size	ReLU
	MaxPool2D, 2x2 kernel size	
	Fully Connected: output size 48	ReLU
	Fully Connected: output size 32	ReLU
	Fully Connected: output size $ z $	ReLU
Q Network	Fully Connected: output size 16	ReLU
	Fully Connected: output size 1	
T Network	Fully Connected: output size 16	ReLU
	Fully Connected: output size $ z $	

Table 2: Learning Rates

Model	Q Loss	L_-	L_+
MF Only	1e-4	0	0
MF + Negative Sampling	1e-4	1e-4	0
MF + Negative & Positive Sampling	1e-4	1e-5	1e-6

A.5 PARAMETERS FOR NETWORK WITH DEEPER Q NETWORK

Module	Layer	Activation
Encoder Network	Conv2D: 16 channels, 2x2 kernel size	ReLU
	Conv2D: 32 channels, 2x2 kernel size	ReLU
	MaxPool2D, 2x2 kernel size	
	Fully Connected: output size 32	ReLU
	Fully Connected: output size $ z $	ReLU
	Fully Connected: output size 32	ReLU
Q Network	Fully Connected: output size 16	ReLU
	Fully Connected: output size 1	
	Fully Connected: output size 16	ReLU
T Network	Fully Connected: output size $ z $	

Table 3: Learning Rates

Model	Q Loss	L_-	L_+
MF Only	1e-4	0	0
MF + Negative Sampling	1e-4	1e-2	0
MF + Negative & Positive Sampling, $\gamma = 0$	1e-4	1e-5	1e-6
MF + Negative & Positive Sampling, $\gamma = 0.25$	1e-4	1e-4	1e-6
MF + Negative & Positive Sampling, $\gamma = 0.5$	1e-4	1e-4	1e-6
MF + Negative & Positive Sampling, $\gamma = 0.8$	1e-4	1e-4	1e-8

A.6 SUPPLEMENTARY FIGURES

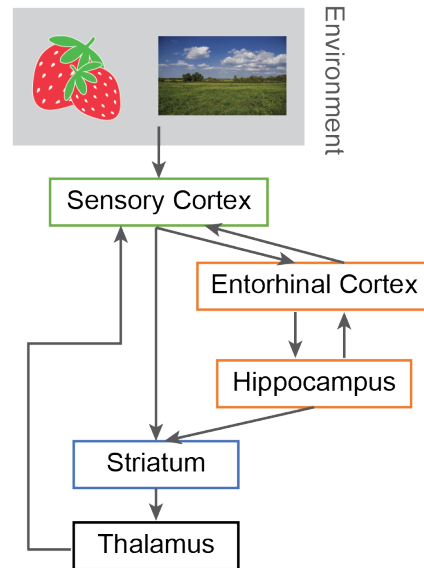


Figure A.1: More accurate and detailed version of anatomy discussed in Figure 1. Although not exhaustive, this diagram shows relevant connections between the regions of interest (Canto et al., 2008; Goodroe et al., 2018; Morgenstern et al., 2022).

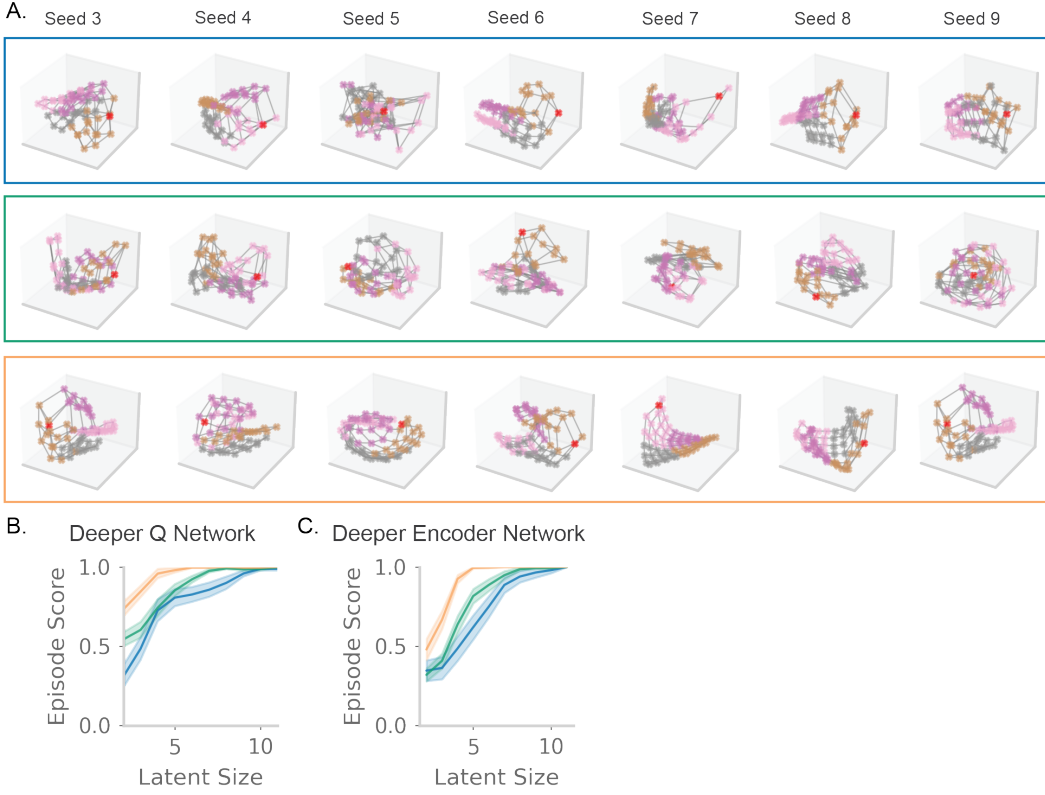


Figure A.2: **A.** As in Figure 2C, but for seven more additional seeds. **B.** As in Figure 2E, but for the model with a deeper Q network. **C.** As in Figure 2E, but for the model with a deeper encoder network.



Figure A.3: **A.** As in Figure 3D, but for six additional seeds, and including $\gamma = 0.8$.

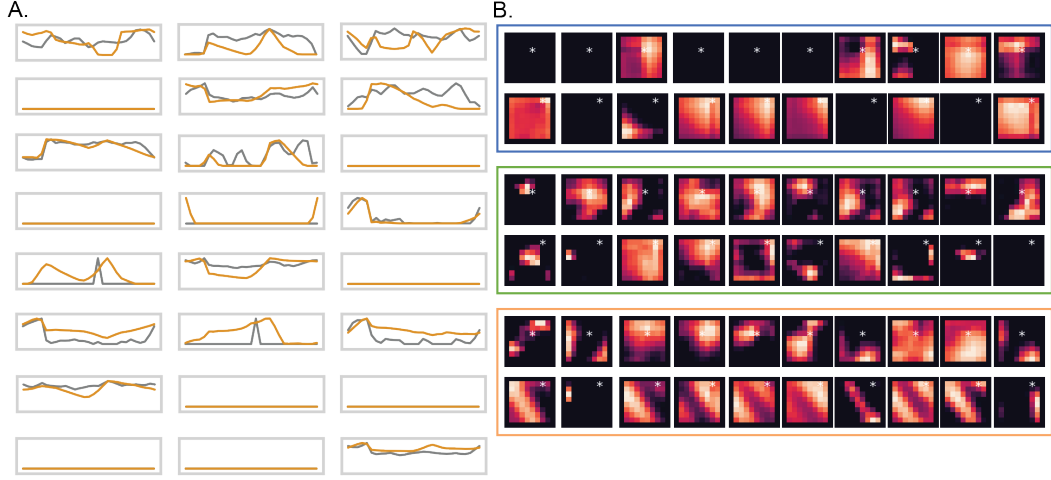


Figure A.4: **A.** As in Figure 4B, but showing all 24 units in a single seed. **B.** As in Figure 4FG, but showing all 10 sorted units (columns) for two additional seeds (rows). In addition, the model with only the negative sampling task is shown (green box).

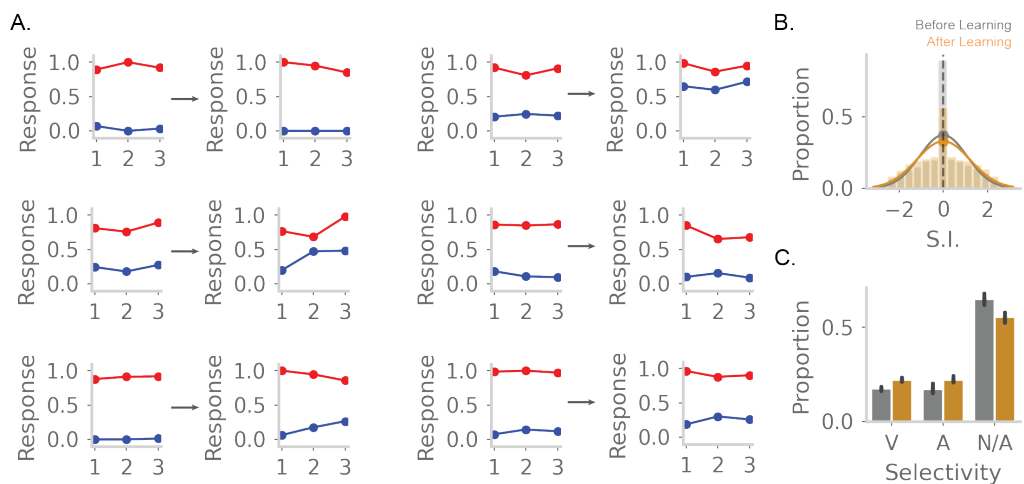


Figure A.5: **A.** As in Figure 5C, but showing six additional units. **B.** As in Figure 5F, but for a model with no value learning head. T-test conducted as in Figure 5F and is not statistically significant (t-statistic: -0.24, p-value: 0.40). **C.** As in Figure 5G, but for a model with no value learning head.